

## Hyperbolic Topological Band Insulators

David M. Urwyler,<sup>1</sup> Patrick M. Lenggenger<sup>1,2,3</sup>, Igor Boettcher<sup>4,5</sup>, Ronny Thomale<sup>6</sup>,  
Titus Neupert<sup>1</sup>, and Tomáš Bzdušek<sup>2,1,\*</sup>

<sup>1</sup>*Department of Physics, University of Zurich, Winterthurerstrasse 190, 8057 Zurich, Switzerland*

<sup>2</sup>*Condensed Matter Theory Group, Paul Scherrer Institute, 5232 Villigen PSI, Switzerland*

<sup>3</sup>*Institute for Theoretical Physics, ETH Zurich, 8093 Zurich, Switzerland*

<sup>4</sup>*Department of Physics, University of Alberta, Edmonton, Alberta T6G 2E1, Canada*

<sup>5</sup>*Theoretical Physics Institute, University of Alberta, Edmonton, Alberta T6G 2E1, Canada*

<sup>6</sup>*Institut für Theoretische Physik und Astrophysik, Universität Würzburg, 97074 Würzburg, Germany*



(Received 23 June 2022; revised 13 October 2022; accepted 26 October 2022; published 8 December 2022)

Recently, hyperbolic lattices that tile the negatively curved hyperbolic plane emerged as a new paradigm of synthetic matter, and their energy levels were characterized by a band structure in a four- (or higher-) dimensional momentum space. To explore the uncharted topological aspects arising in hyperbolic band theory, we here introduce elementary models of hyperbolic topological band insulators: the hyperbolic Haldane model and the hyperbolic Kane-Mele model; both obtained by replacing the hexagonal cells of their Euclidean counterparts by octagons. Their nontrivial topology is revealed by computing topological invariants in both position and momentum space. The bulk-boundary correspondence is evidenced by comparing bulk and boundary density of states, by modeling propagation of edge excitations, and by their robustness against disorder.

DOI: [10.1103/PhysRevLett.129.246402](https://doi.org/10.1103/PhysRevLett.129.246402)

*Introduction.*—The interplay between the crystal structure of materials and their electronic band-structure topology is pivotal to modern condensed matter physics, with major recent developments in areas such as topological quantum chemistry [1–3] and moiré materials [4]. With the ground-breaking experimental realization of hyperbolic lattices in coupled waveguide resonators [5] and electric-circuit networks [6], such exotic lattices have been elevated from purely mathematical objects [7,8] to promising tabletop platforms for simulating quantum many-body physics in curved space. These experimental achievements have also inspired numerous theoretical studies of hyperbolic lattices. Notably, hyperbolic band theory (HBT) has been formulated [9], enabling the characterization of their energy spectra via band structures in momentum space. The range of recently investigated physical phenomena further includes the effects of magnetic fields [10–12], continuum approximation [13], periodic boundary conditions [14–16], hyperbolic crystallography [17], photon bound states [18], exact trace formulas [19], Bose-Hubbard model [15], elastic vibrations [20], and flat bands [21–24]. Notably, two very recent works proposed concrete models of hyperbolic topological insulators [25,26]; however, a systematic investigation of topological quantum numbers on hyperbolic lattices remains largely unexplored.

Among the multitude of hyperbolic lattices, which are tessellations of the two-dimensional (2D) hyperbolic plane of negative curvature [27], the so-called  $\{8, 3\}$  lattice presents a unique opportunity for a first systematic study

of band topology in toy models with topological ground states. The graph of this lattice consists of regular octagons with three lines meeting at each vertex. Hence it derives from the honeycomb lattice (denoted  $\{6, 3\}$  in this context) through replacing hexagons by octagons. Importantly, HBT predicts that the Brillouin zone (BZ) of this lattice is four-dimensional (4D) [17], with crystal momentum  $\mathbf{k} = (k_1, k_2, k_3, k_4)$ , separating the dimensions of position and momentum space as a genuine property of hyperbolic lattices. This enhanced dimensionality suggests [28,29] that hyperbolic models may host larger families of strong and weak topological band insulators than their Euclidean counterparts.

In this Letter, we introduce two elemental models of hyperbolic topological band insulators, the hyperbolic Haldane and hyperbolic Kane-Mele (KM) models on the  $\{8, 3\}$  lattice, which generalize the quintessential namesake Euclidean models formulated on the  $\{6, 3\}$  lattice [30–34]. These models could be implemented experimentally using the platforms of Refs. [5,6,35–37]. Importantly, due to the applicability of both HBT and real-space topological markers [38–42] on the  $\{8, 3\}$  lattice, we are able to study band-topological properties in both position and momentum space. This dual point of view allows us to compare topological invariants of hyperbolic topological insulators in momentum and position space, and to study their associated bulk-boundary correspondence. Our models and analysis surpass the study of hyperbolic Hofstadter and Haldane-like models in Refs. [10,25,26] as they do not utilize the complementary momentum-space picture.

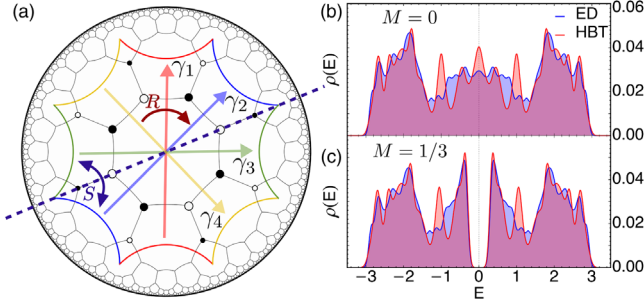


FIG. 1. Nearest-neighbor model on the  $\{8, 3\}$  lattice. (a) The lattice consists of octagons with coordination number three. The Bolza cell (multicolored octagon), the fundamental tile of the hyperbolic Bravais lattice, contains six elementary octagons and 16 sites (black and white dots). The colored arrows labeled  $\gamma_1, \dots, \gamma_4$  are the generators of the hyperbolic Bravais lattice. Rotation  $R$  (dark red) and reflection  $S$  (dark blue) are symmetries of the model. (b),(c) Bulk density of states  $\rho(E)$  for the nearest-neighbor model on the  $\{8, 3\}$ -lattice, extracted from hyperbolic band theory (HBT, red) vs. exact diagonalization (ED, blue) in the absence (b) vs presence (c) of a sublattice potential  $M$ .

*Tight-binding models.*—We consider models on the hyperbolic  $\{8, 3\}$  lattice, which is comprised of octagonal faces with three lines meeting at each vertex, see Fig. 1(a). This lattice consists of a 16-site unit cell that is repeated infinitely many times according to a hyperbolic Bravais lattice, which is the  $\{8, 8\}$  lattice in this case [17], comprised of octagonal plaquettes with coordination number eight. We refer to the unit cell as the *Bolza cell*—a name inspired by the fact that this cell covers the Bolza surface (the most symmetric genus-two Riemann surface [43]). The Bravais lattice is generated by four noncommuting hyperbolic translations, denoted  $\gamma_1, \dots, \gamma_4$ .

To obtain the energy bands for a tight-binding model with nearest-neighbor (NN) hopping on the  $\{8, 3\}$  lattice from HBT, the Bolza cell is equipped with twisted boundary conditions [9], defined by four phase factors,  $e^{ik_1}, \dots, e^{ik_4}$ , along the directions of the four generators: each bond crossing one of the eight sides of the Bolza cell acquires a phase factor. This yields a  $16 \times 16$  *hyperbolic Bloch Hamiltonian*  $\mathcal{H}_{\text{Bloch}}(\mathbf{k})$ , whose eigenvalues comprise 16 energy bands of the  $\{8, 3\}$  lattice in 4D momentum space. We henceforth set the NN hopping parameter to unity.

The density of states (DOS) of tight-binding models,  $\rho(E)$ , can be obtained either (i) through exact diagonalization (ED) on finite hyperbolic graphs, or (ii) via HBT by sampling  $\mathbf{k}$  over the 4D BZ. We refer to finite hyperbolic graphs with open boundary as *flakes*. To remove the contribution of boundary states, we define in ED calculations the *bulk-DOS* as the sum of local-DOS on the 16 sites in the innermost Bolza cell [44]. Whether the two just-defined DOS functions should match for large systems remains at present an open problem, since HBT only identifies eigenstates transforming in Abelian representations of the

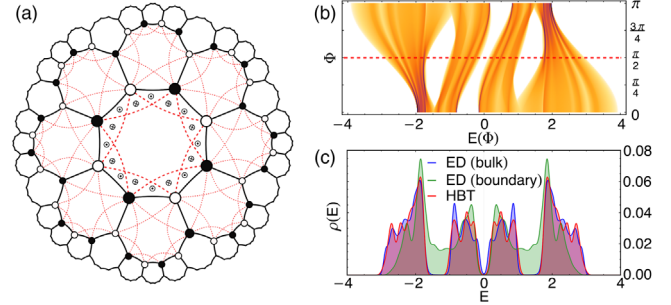


FIG. 2. Hyperbolic Haldane model. (a) Schematic depiction of the model. Red dashed lines indicate next-to-nearest neighbor hopping with amplitude  $t_2 e^{\pm i\Phi}$ . The phases  $\pm\Phi$  arise due to alternating magnetic fluxes [symbols  $\odot$  ( $\otimes$ ) in the innermost octagon] through the system. (b) Density of states for  $t_2 = M/2 = \frac{1}{6}$  computed from HBT, revealing three energy gaps. (c) Bulk-DOS functions  $\rho^{\text{HBT}}(E)$  and  $\rho_{\text{bulk}}^{\text{ED}}(E)$  for  $\Phi = \pi/2$  (red dashed line in b) computed using HBT (red) and ED (blue), and the boundary-DOS  $\rho_{\text{boundary}}^{\text{ED}}$  (green).

noncommutative translation group [45]. Nevertheless, the results for the NN model, compared in Fig. 1(b), indicate an auspicious level of agreement, with the deviations partly attributable to residual boundary effects [46].

We next consider the inclusion of an on-site potential  $\pm M$  with opposite sign on the two sublattices of the  $\{8, 3\}$  lattice, marked with white and black in Fig. 1(a). In the absence of a sublattice potential, the DOS is gapless at  $E = 0$ , whereas we observe a gap  $\Delta E = 2M$  for  $M \neq 0$ . This feature is reproduced both with ED and HBT. In fact, for all tight-binding models studied in this work, whenever HBT predicts a gap in the DOS at certain energies, then a bulk gap is also found in this energy range with ED on flakes. Whether this behavior generalizes to all hyperbolic lattice models constitutes a formidable question for future investigations.

*Topological band insulators.*—We introduce the *hyperbolic Haldane model* on the  $\{8, 3\}$  lattice by including complex-valued next-to-nearest-neighbor hopping terms,  $t_2 e^{\pm i\Phi}$ , to the tight-binding Hamiltonian of the previous section. The positive (negative) sign is chosen in the exponent for hopping in the clockwise (counterclockwise) direction within an octagon. This model describes spinless fermions coupled orbitally to staggered magnetic fluxes, see Fig. 2(a). The associated Bloch Hamiltonian  $\mathcal{H}_H(\mathbf{k})$  with crystal momentum  $\mathbf{k} = (k_1, k_2, k_3, k_4)$  is constructed using HBT [44]. The magnetic field breaks time-reversal symmetry, locating the model in Altland-Zirnbauer class A [28,47]; we therefore anticipate that its topology is encoded by the Chern class [29,48].

We investigate in Fig. 2(b) the model in terms of the DOS function  $\rho^{\text{HBT}}(E; \Phi)$  as  $\Phi$  is varied for  $t_2 = M/2 = 1/6$ . We identify extended gapped regions at filling fractions  $f = 5/16, 8/16, 11/16$ , corresponding, respectively, to chemical potentials  $\mu = -1.3, 0, 1.3$  at  $\Phi = \pi/2$ .

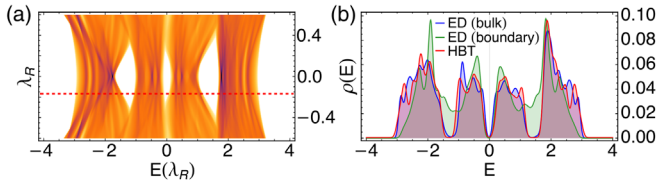


FIG. 3. Hyperbolic Kane-Mele model. (a) Density of states for  $t_2 = M/2 = \frac{1}{6}$  computed from HBT, which reveals three energy gaps at small Rashba coupling  $\lambda_R$ . (b) Bulk-DOS functions for  $\lambda_R = -\frac{1}{6}$  (red dashed line in (a)) computed using HBT (red) and ED (blue), and the boundary-DOS function (green).

(In contrast to the Euclidean case, nonvanishing  $M \neq 0$  is necessary to open an energy gap at half-filling for the hyperbolic Haldane model [44].) In Fig. 2(c) we observe that the bulk gaps extracted from ED on flakes and from HBT again agree. Two of the three gaps are special in that they are filled by boundary states, as is inferred from ED by integrating the local-DOS over boundary sites [44]. Below, we reveal that these energy gaps are associated with nontrivial Chern topology and chiral edge states.

Next we introduce the *hyperbolic Kane-Mele (KM) model* of spin- $\frac{1}{2}$  fermions on the  $\{8, 3\}$  lattice as a time-reversal-symmetric topological model in Altland-Zimbauer class AII. The model can be interpreted as a “doubled” version of the Haldane model, graded with a spin degree of freedom, in the following sense [31,49]: denoting the Hamiltonian of the Haldane model by  $\mathcal{H}_H$ , the Kane-Mele Hamiltonian for the spin-up (spin-down) fermions reads  $\mathcal{H}_H$  ( $\mathcal{H}_H^*$ ), and is supplied with spin-mixing Rashba term with amplitude  $\lambda_R$ . Since the hyperbolic curvature induces nontrivial holonomy of the spin along closed loops of the lattice, constructing a symmetry-compatible Rashba term is challenging. We therefore simplify the model here by assuming a nonconstant curvature that is concentrated at the corners of the Bolza cell, while the curvature is flat everywhere else (for detailed construction see Supplemental Material Fig. S1 [44]). We call this simplified model the *reduced hyperbolic KM model*.

The reduced KM model is expected to exhibit energy gaps at the same filling fractions as the Haldane model as long as  $\lambda_R$  is sufficiently small. This is verified by the plot of  $\rho^{\text{HBT}}(E; \lambda_R)$  in Fig. 3(a). The obtained data motivate us to fix  $\lambda_R = -1/6$ , in which case all three gaps are still present. The comparison of the resulting  $\rho^{\text{HBT}}(E)$  and  $\rho_{\text{bulk}}^{\text{ED}}(E)$  is shown in Fig. 3(b). The same panel also displays the corresponding  $\rho_{\text{boundary}}^{\text{ED}}(E)$ , which reveals filling of the two outer energy gaps by edge states, portending a nontrivial Kane-Mele topology.

*Topological invariants.*—We compute topological invariants in momentum and position space for the band gaps of both constructed models. In momentum space, we compute the first Chern numbers of the Haldane model from the Bloch Hamiltonian  $\mathcal{H}_H(\mathbf{k})$  in the six planes spanned by

TABLE I. Values of topological invariants for the considered hyperbolic models, with the three energy gaps labeled by their filling fraction ( $f$ ) and chemical potential ( $\mu$ ).

$f$	$\mu$	Haldane				Kane-Mele			
		$\mathcal{C}_a$	$\mathcal{C}_b$	$\mathcal{C}_c$	$\mathcal{C}_{\text{RS}}$	$\nu_a$	$\nu_b$	$\nu_c$	$\nu_{\text{RS}}$
5/16	-1.3	-1	+1	-1	-0.986	1	1	1	-0.971
8/16	0	0	0	0	0	0	0	0	0
11/16	+1.3	-1	+1	-1	-0.986	1	1	1	-0.971

pairs  $(k_i, k_j)$  of momentum components,  $i, j = 1, \dots, 4$ . The model exhibits  $(\pi/2)$ -rotation symmetry  $R$  around the center of the Bolza cell [dark red arrow in Fig. 1(a)], which transforms the group generators as  $(\gamma_1, \gamma_2, \gamma_3, \gamma_4) \mapsto (\gamma_3, \gamma_4, \gamma_1^{-1}, \gamma_2^{-1})$ ; therefore, the Hamiltonians  $\mathcal{H}_H(k_1, k_2, k_3, k_4)$  and  $\mathcal{H}_H(k_3, k_4, -k_1, -k_2)$  are related by a unitary transformation. Consequently, one can relate Chern numbers  $\mathcal{C}_{12} = \mathcal{C}_{34} =: \mathcal{C}_a$  and  $\mathcal{C}_{14} = \mathcal{C}_{23} =: \mathcal{C}_c$ . In addition, while reflection  $S$  [dashed blue line in Fig. 1(a)] flips the magnetic fluxes  $\pm\Phi$ , its composition with time-reversal constitutes an antiunitary symmetry of the Haldane model, transforming  $(k_1, k_2, k_3, k_4) \mapsto (-k_4, -k_3, -k_2, -k_1)$  and relating  $\mathcal{C}_{13} = \mathcal{C}_{24} =: \mathcal{C}_b$ . We compute  $\mathcal{C}_{a,b,c}$  using Wilson loops [50,51], and find that energy gaps at  $f = 5/16, 11/16$  have nontrivial Chern number  $\pm 1$  in all planes, while the gap at  $f = 8/16$  does not exhibit Chern topology, see Table I. Similarly, after utilizing the  $R$  and  $S$  symmetry of  $\mathcal{H}_{\text{KM}}(\mathbf{k})$ , we identify three independent  $\mathbb{Z}_2$ -topological invariants  $\nu_{ij}$ , namely,  $\nu_a := \nu_{12} = \nu_{34}$ ,  $\nu_b := \nu_{13} = \nu_{24}$ , and  $\nu_c := \nu_{14} = \nu_{23}$ . We find that  $\nu_{a,b,c}$  are all nontrivial for the two outer band gaps, while they are trivial for the inner gap, see Table I. [We discuss in the Supplemental Material [44] that if  $M = 0$  then an additional  $(\pi/4)$ -rotation symmetry further implies  $\mathcal{C}_a = \mathcal{C}_c$  and  $\nu_a = \nu_c$ ].

We also computed higher-dimensional topological invariants for  $\mathcal{H}_H(\mathbf{k})$  and  $\mathcal{H}_{\text{KM}}(\mathbf{k})$ , namely, the  $\mathbb{Z}_2$ -valued Fu-Kane-Mele invariant [52] on 3D subspaces (for KM) and the second Chern number [48,53] in 4D BZ (for both). These, however, are all trivial. Nevertheless, hyperbolic toy models with nonvanishing values of such topological invariants could be constructed through reverse engineering: starting from a 4D Euclidean Bloch-Hamiltonian,  $\mathcal{H}_{\text{Euc}}(\mathbf{k})$ , which features such topological invariants, one constructs a hyperbolic tight-binding model where each component  $k_i$  of  $\mathbf{k}$  is replaced by a generator  $\gamma_i$  of the hyperbolic Bravais lattice. We leave this promising route for designing topological hyperbolic Hamiltonians for future research.

We complement the momentum-space discussion of the band topology of the two models with real-space topological markers [38–42]. Importantly, these computations include states transforming in *all* representations of the noncommutative translation group, hence going beyond HBT. For the Haldane model, we compute the *real-space Chern number*  $\mathcal{C}_{\text{RS}}$  as introduced in Ref. [39] (detailed in

Supplemental Material [44]). This algorithm does not warrant quantized results, but we confirm that integers are approached as the summation regions are enlarged. Our position-space analysis confirms that the energy gaps at  $\mu = \pm 1.3$  are topological, while the one at  $\mu = 0$  is trivial, see Table I. We observe  $C_{RS} = C_a = -C_b = C_c$  for all phases with gapped bulk. Recall here that for 2D Euclidean lattices we have  $C_{RS} = C_{12}$  [38,39], whereas no exact relation is currently known for hyperbolic lattices.

We further adapt the techniques of Refs. [39–42] to compute the *real-space spin Chern number*  $\nu_{RS} \in \mathbb{Z}$  of the reduced KM model for each bulk gap. This invariant is integer-valued as long as spin-mixing terms in the Hamiltonian are sufficiently weak, and for Euclidean lattice models it obeys  $\nu_{RS} = \nu_{12} \pmod{2}$  [41,42]. We observe that the extracted  $\mathbb{Z}_2$  invariants obey  $\nu_{RS} = \nu_a = \nu_b = \nu_c \pmod{2}$  for all cases analyzed. Whether there exists a simple *universal* relation between the parities of  $\nu_{a,b,c,RS}$  constitutes another open question.

*Bulk-boundary correspondence.*—We finally investigate whether the nontrivial band topology identified in the bulk for both models is reflected in topological edge states on the boundary. For this, we (i) extract the edge-state dispersion, (ii) showcase the propagation of an edge-localized wave packet around the flake boundary, and (iii) investigate their robustness against disorder.

(i) When computing for a circular flake the edge-state dispersion ( $E$ ) against angular momentum ( $\ell$ ), note that the latter is only defined modulo 4 due to the fourfold-rotation symmetry  $R$ . To obtain  $E(\ell)$  for *unbounded*  $\ell \in \mathbb{Z}$ , we decompose the lattice eigenstates  $|\phi_j\rangle$  into eigenmodes  $|\psi_{n,\ell}\rangle$  of the Laplace-Beltrami operator defined in the continuum [6,13] and select the number  $\ell$  with the largest contribution (for details see Supplemental Material [44]). We plot  $E(\ell)$  for the edge states in the hyperbolic Haldane model for the energy gap at  $\mu = 1.3$  in Fig. 4(a). We observe a single dispersive branch for positive  $\ell$  only, implying chiral edge state at the flake boundary, in agreement with  $|C_{RS}| = 1$ . An analogous analysis for the reduced Kane-Mele model at the same filling reveals a pair of counterpropagating *helical* branches, compatible with  $|\nu_{RS}| = 1$  (see Supplemental Material Fig. S7 [44]).

(ii) To study the propagation of a *wave packet* along the edge, we construct a boundary-localized Gaussian state with energy near  $\mu$  and with energy width  $\sigma$  [44]. We plot in Figs. 4(b) and 4(c) the time-evolution of a wave packet initialized with parameters  $(\mu, \sigma) = (1.3, 0.025)$  in the hyperbolic Haldane model. We find the center of the packet smoothly propagates along the boundary in time. The angular group velocity of the wave packet extracted from the time evolution matches the edge dispersion from (i) via  $\omega_{\text{group}} = dE/d\ell$ . We similarly analyzed the edge-state propagation for the reduced KM model [44] and confirmed their anticipated helical character.

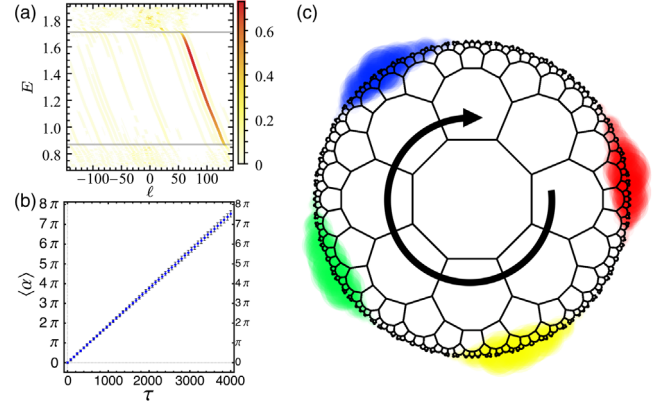


FIG. 4. Topological edge states. (a) Edge-dispersion  $E$  as a function of angular momentum  $\ell$  for chiral edge states in the upper energy gap of the hyperbolic Haldane model. (b) Propagation of a Gaussian wave packet along the flake boundary;  $\langle \alpha \rangle$  is the angular displacement in time  $\tau$ , and error bars indicate the width of the wave packet. (c) Snapshots of the wave packet at  $\tau = 0, 240, 480, 720$  (colored, respectively, red, yellow, green, and blue). The area of a disk centered at a given site encodes the probability to find the particle at that site.

(iii) To quantify the robustness of the edge states against Anderson localization when subject to disorder, we show that they retain a small *inverse participation ratio* (IPR). Here  $0 < \text{IPR} \leq 1$  is defined such that an eigenstate  $|\phi_j\rangle$  characterized by value  $\text{IPR}_j$  has most support over approximately  $1/\text{IPR}_j$  sites [44]. For the reduced KM model, we add random spin-mixing terms that either preserve (TRS) or break (TRB) time-reversal symmetry of the model. These can be interpreted as *random Rashba terms* and *random*

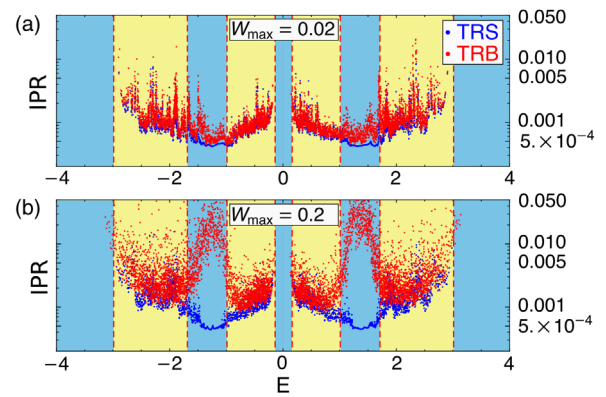


FIG. 5. Robustness against Anderson localization. For the reduced hyperbolic KM model, we consider inclusion of random spin-mixing terms that preserve (TRS, blue) or break (TRB, red) time-reversal symmetry. A dot with coordinates  $(E_j, \text{IPR}_j)$  represents the energy and the inverse participation ratio of an eigenstate  $|\phi_j\rangle$  in the flake geometry. The random terms are drawn from a uniform distribution with  $W_{\text{max}} = 0.02$  (a) and  $W_{\text{max}} = 0.2$  (b). The blue (yellow) backgrounds indicate energy ranges corresponding to bulk gap (bulk band) in the absence of disorder.

*magnetic fields*, respectively, with an amplitude  $W \in [-W_{\max}, W_{\max}]$  drawn from a uniform distribution. The results in Fig. 5 indicate that disorder with TRB leads to localization of the edge states, whereas increasing  $W_{\max}$  in the presence of TRS does not change their IPR values significantly, as expected for topological edge states. We similarly verified for the hyperbolic Haldane model that inclusion of random on-site potential drawn from a uniform distribution  $W \in [-W_{\max}, W_{\max}]$  has little effect on the IPR of the edge states. In addition, we confirmed that the chiral propagation of the edge states without backscattering is preserved under the addition of the random terms (see Supplemental Material Fig. S4 [44]). This provides further evidence of the nontrivial topology of the constructed model.

*Outlook.*—Our work constitutes an essential step towards designing topological hyperbolic Hamiltonians and exploring the interplay of geometry and topology in such systems. It is natural to wonder if similar constructions of topological insulators generalize to other hyperbolic  $\{p, q\}$  lattices. Indeed, the Haldane model on the  $\{6, 4\}$  lattice has very recently been implemented as an electric-circuit network by Ref. [25], while another model of Chern insulator on the  $\{8, 3\}$  lattice, although lacking translation symmetry, has been considered by Ref. [26]. However, these works did not apply HBT to characterize the models, thus lacking the momentum-space language.

A key difference between hyperbolic and Euclidean lattices is the extensive scaling of the boundary in the hyperbolic case, implying a finite fraction of sites are at the boundary *irrespective* of the system size [13,22]. Consequently, a *macroscopic fraction of all states* contributes to topological edge modes, in stark contrast to Euclidean topological models. It will be intriguing to investigate features of non-Hermitian topology in this context, as the non-Hermitian skin effect likewise affects a macroscopic fraction of the spectrum [54–59]. The extensive hyperbolic boundary is also anticipated to give access to novel one-dimensional many-body models affected by the bulk design through the bulk-boundary correspondence.

The Wolfram Language code and the generated data used to arrive at the conclusions presented in this work are publicly available in Ref. [60]. The manuscript is based on the master’s thesis of one of the authors [49].

We would like to express our thanks to M. Brzezińska, A. Chen, B. Lapierre, J. Maciejko, A. Stegmaier, T. Tummuru, and L. K. Upreti for helpful discussions. P. M. L. and T. B. were supported by the Ambizione Grant No. 185806 by the Swiss National Science Foundation. I. B. acknowledges support from the University of Alberta startup fund UOFAB Startup Boettcher and the Natural Sciences and Engineering Research Council of Canada (NSERC) Discovery Grants No. RGPIN-2021-02534 and

No. DGEER2021-00043. R. T. acknowledges funding by the Deutsche Forschungsgemeinschaft (DFG, German Research Foundation) through Project-ID 258499086—SFB 1170, and through the Würzburg-Dresden Cluster of Excellence on Complexity and Topology in Quantum Matter—*ct.qmat* Project-ID 39085490—EXC 2147. T. N. acknowledges support from the European Research Council (ERC) under the European Union’s Horizon 2020 research and innovation program (ERC-StG-Neupert-757867-PARATOP).

\*Corresponding author.  
tomas.bzdusek@psi.ch

- [1] Barry Bradlyn, L. Elcoro, Jennifer Cano, M. G. Vergniory, Zhijun Wang, C. Felser, M. I. Aroyo, and B. Andrei Bernevig, Topological quantum chemistry, *Nature (London)* **547**, 298 (2017).
- [2] Hoi Chun Po, Ashvin Vishwanath, and Haruki Watanabe, Symmetry-based indicators of band topology in the 230 space groups, *Nat. Commun.* **8**, 50 (2017).
- [3] Maia G. Vergniory, Benjamin J. Wieder, Luis Elcoro, Stuart S. P. Parkin, Claudia Felser, B. Andrei Bernevig, and Nicolas Regnault, All topological bands of all nonmagnetic stoichiometric materials, *Science* **376**, abg9094 (2022).
- [4] Eva Y. Andrei, Dmitri K. Efetov, Pablo Jarillo-Herrero, Allan H. MacDonald, Kin Fai Mak, T. Senthil, Emanuel Tutuc, Ali Yazdani, and Andrea F. Young, The marvels of moiré materials, *Nat. Rev. Mater.* **6**, 201 (2021).
- [5] Alicia J. Kollár, Mattias Fitzpatrick, and Andrew A. Houck, Hyperbolic lattices in circuit quantum electrodynamics, *Nature (London)* **571**, 45 (2019).
- [6] Patrick M. Lenggenhager, Alexander Stegmaier, Lavi K. Upreti, Tobias Hofmann, Tobias Helbig, Achim Vollhardt, Martin Greiter, Ching Hua Lee, Stefan Imhof, Hauke Brand, Tobias Kießling, Igor Boettcher, Titus Neupert, Ronny Thomale, and Tomáš Bzdusek, Simulating hyperbolic space on a circuit board, *Nat. Commun.* **13**, 4373 (2022).
- [7] W. Magnus, *Noneuclidean Tesselations and Their Groups* (Academic Press, New York, 1974).
- [8] H. S. M. Coxeter and W. O. J. Moser, *Generators and Relations for Discrete Groups* (Springer Berlin Heidelberg, Berlin, Heidelberg, 1980).
- [9] Joseph Maciejko and Steven Rayan, Hyperbolic band theory, *Sci. Adv.* **7**, eabe9170 (2021).
- [10] Sunkyu Yu, Xianji Piao, and Namkyoo Park, Topological Hyperbolic Lattices, *Phys. Rev. Lett.* **125**, 053901 (2020).
- [11] Kazuki Ikeda, Shoto Aoki, and Yoshiyuki Matsuki, Hyperbolic band theory under magnetic field and Dirac cones on a higher genus surface, *J. Phys. Condens. Matter* **33**, 485602 (2021).
- [12] Alexander Stegmaier, Lavi K. Upreti, Ronny Thomale, and Igor Boettcher, Universality of Hofstadter Butterflies on Hyperbolic Lattices, *Phys. Rev. Lett.* **128**, 166402 (2022).
- [13] Igor Boettcher, Przemyslaw Bienias, Ron Belyansky, Alicia J. Kollár, and Alexey V. Gorshkov, Quantum simulation of hyperbolic space with circuit quantum electrodynamics: From graphs to geometry, *Phys. Rev. A* **102**, 032208 (2020).

- [14] Joseph Maciejko and Steven Rayan, Automorphic Bloch theorems for hyperbolic lattices, *Proc. Natl. Acad. Sci. U.S.A.* **119**, e2116869119 (2022).
- [15] Xingchuan Zhu, Jiaojiao Guo, Nikolas P. Breuckmann, Huaiming Guo, and Shiping Feng, Quantum phase transitions of interacting bosons on hyperbolic lattices, *J. Phys. Condens. Matter* **33**, 335602 (2021).
- [16] Nikolas P. Breuckmann and Barbara M. Terhal, Constructions and noise threshold of hyperbolic surface codes, *IEEE Trans. Inf. Theory* **62**, 3731 (2016).
- [17] Igor Boettcher, Alexey V. Gorshkov, Alicia J. Kollár, Joseph Maciejko, Steven Rayan, and Ronny Thomale, Crystallography of hyperbolic lattices, *Phys. Rev. B* **105**, 125118 (2022).
- [18] Przemyslaw Bienias, Igor Boettcher, Ron Belyansky, Alicia J. Kollár, and Alexey V. Gorshkov, Circuit Quantum Electrodynamics in Hyperbolic Space: From Photon Bound States to Frustrated Spin Models, *Phys. Rev. Lett.* **128**, 013601 (2022).
- [19] Adil Attar and Igor Boettcher, Selberg trace formula in hyperbolic band theory, *Phys. Rev. E* **106**, 034114 (2022).
- [20] Massimo Ruzzene, Emil Prodan, and Camelia Prodan, Dynamics of elastic hyperbolic lattices, *Extreme Mech. Lett.* **49**, 101491 (2021).
- [21] Alicia J. Kollár, Mattias Fitzpatrick, Peter Sarnak Sarnak, and Andrew A. Houck, Line-graph lattices: Euclidean and non-Euclidean flat bands, and implementations in circuit quantum electrodynamics, *Commun. Math. Phys.* **376**, 1909 (2019).
- [22] Alberto Saa, Eduardo Miranda, and Francisco Rouxinol, Higher-dimensional Euclidean and non-Euclidean structures in planar circuit quantum electrodynamics, [arXiv: 2108.08854](https://arxiv.org/abs/2108.08854).
- [23] Tomáš Bzdušek and Joseph Maciejko, Flat bands and band-touching from real-space topology in hyperbolic lattices, *Phys. Rev. B* **106**, 155146 (2022).
- [24] Rémy Mosseri, Roger Vogeler, and Julien Vidal, Aharonov-Bohm cages, flat bands, and gap labeling in hyperbolic tilings, *Phys. Rev. B* **106**, 155120 (2022).
- [25] Weixuan Zhang, Hao Yuan, Na Sun, Houjun Sun, and Xiangdong Zhang, Observation of novel topological states in hyperbolic lattices, *Nat. Commun.* **13**, 2937 (2022).
- [26] Zheng-Rong Liu, Chun-Bo Hua, Tan Peng, and Bin Zhou, Chern insulator in a hyperbolic lattice, *Phys. Rev. B* **105**, 245301 (2022).
- [27] Svetlana Katok, *Fuchsian Groups* (University of Chicago Press, Chicago, 1992).
- [28] Alexei Kitaev, Periodic table for topological insulators and superconductors, *AIP Conf. Proc.* **1134**, 22 (2009).
- [29] Shinsei Ryu, Andreas P. Schnyder, Akira Furusaki, and Andreas W. W. Ludwig, Topological insulators and superconductors: Tenfold way and dimensional hierarchy, *New J. Phys.* **12**, 065010 (2010).
- [30] F. D. M. Haldane, Model for a Quantum Hall Effect without Landau Levels: Condensed-Matter Realization of the “Parity Anomaly”, *Phys. Rev. Lett.* **61**, 2015 (1988).
- [31] C. L. Kane and E. J. Mele,  $Z_2$  Topological Order and the Quantum Spin Hall Effect, *Phys. Rev. Lett.* **95**, 146802 (2005).
- [32] Alexander B. Khanikaev, S. Hossein Mousavi, Wang-Kong Tse, Mehdi Kargarian, Allan H. MacDonald, and Gennady Shvets, Photonic topological insulators, *Nat. Mater.* **12**, 233 (2013).
- [33] Gregor Jotzu, Michael Messer, Rémi Desbuquois, Martin Lebrat, Thomas Uehlinger, Daniel Greif, and Tilman Esslinger, Experimental realization of the topological Haldane model with ultracold fermions, *Nature (London)* **515**, 237 (2014).
- [34] Yujiang Ding, Yugui Peng, Yifan Zhu, Xudong Fan, Jing Yang, Bin Liang, Xuefeng Zhu, Xiangang Wan, and Jianchun Cheng, Experimental Demonstration of Acoustic Chern Insulators, *Phys. Rev. Lett.* **122**, 014302 (2019).
- [35] Stefan Imhof, Christian Berger, Florian Bayer, Johannes Brehm, Laurens W. Molenkamp, Tobias Kiessling, Frank Schindler, Ching Hua Lee, Martin Greiter, Titus Neupert, and Ronny Thomale, Topoelectrical-circuit realization of topological corner modes, *Nat. Phys.* **14**, 925 (2018).
- [36] Ching Hua Lee, Stefan Imhof, Christian Berger, Florian Bayer, Johannes Brehm, Laurens W. Molenkamp, Tobias Kiessling, and Ronny Thomale, Topoelectrical circuits, *Commun. Phys.* **1**, 39 (2018).
- [37] Tobias Hofmann, Tobias Helbig, Ching Hua Lee, Martin Greiter, and Ronny Thomale, Chiral Voltage Propagation and Calibration in a Topoelectrical Chern Circuit, *Phys. Rev. Lett.* **122**, 247702 (2019).
- [38] J. Bellissard, A. van Elst, and H. Schulz-Baldes, The noncommutative geometry of the quantum Hall effect, *J. Math. Phys. (N.Y.)* **35**, 5373 (1994).
- [39] Alexei Kitaev, Anyons in an exactly solved model and beyond, *Ann. Phys. (Amsterdam)* **321**, 2 (2006).
- [40] Raffaello Bianco and Raffaele Resta, Mapping topological order in coordinate space, *Phys. Rev. B* **84**, 241106(R) (2011).
- [41] Emil Prodan, Disordered topological insulators: A noncommutative geometry perspective, *J. Phys. A Math. Theor.* **44**, 113001 (2011).
- [42] Huaqing Huang and Feng Liu, Theory of spin Bott index for quantum spin Hall states in nonperiodic systems, *Phys. Rev. B* **98**, 125130 (2018).
- [43] M. E. Kazaryan, S. K. Lando, and V. V. Prasolov, *Algebraic Curves: Towards Moduli Spaces*, Moscow Lectures (Springer, Cham, Switzerland, 2019), Vol. 2.
- [44] See Supplemental Material at <http://link.aps.org/supplemental/10.1103/PhysRevLett.129.246402> for supporting data and detailed information about the methods.
- [45] Nan Cheng, Francesco Serafin, James McInerney, Zeb Rocklin, Kai Sun, and Xiaoming Mao, Band Theory and Boundary Modes of High-Dimensional Representations of Infinite Hyperbolic Lattices, *Phys. Rev. Lett.* **129**, 088002 (2022).
- [46] Anffany Chen, Hauke Brand, Tobias Helbig, Tobias Hofmann, Stefan Imhof, Alexander Fritzsche, Tobias Kießling, Alexander Stegmaier, Lavi K. Upreti, Titus Neupert, Tomáš Bzdušek, Martin Greiter, Ronny Thomale, and Igor Boettcher, Hyperbolic matter in electrical circuits with tunable complex phases, [arXiv:2205.05106](https://arxiv.org/abs/2205.05106).
- [47] Alexander Altland and Martin R. Zirnbauer, Nonstandard symmetry classes in mesoscopic normal-superconducting hybrid structures, *Phys. Rev. B* **55**, 1142 (1997).

- [48] Mikio Nakahara, *Geometry, Topology and Physics*, Graduate student series in physics (Hilger, Bristol, 1990).
- [49] David M. Urwyler, Hyperbolic Topological Insulator, Master's thesis, University of Zürich, Switzerland, 2021, [10.13140/RG.2.2.34715.34081](https://doi.org/10.13140/RG.2.2.34715.34081); David M. Urwyler, Patrick M. Lenggenger, Titus Neupert, and Tomáš Bzdušek, Topological hyperbolic band insulators, *APS March Meeting 2022*, Session N66 (2022), <https://meetings.aps.org/Meeting/MAR22/Session/N66.7>.
- [50] Alexey A. Soluyanov and David Vanderbilt, Computing topological invariants without inversion symmetry, *Phys. Rev. B* **83**, 235401 (2011).
- [51] Dominik Gresch, Gabriel Autès, O. V. Yazyev, Matthias Troyer, David Vanderbilt, B. A. Bernevig, and A. A. Soluyanov, Z2Pack: Numerical implementation of hybrid Wannier centers for identifying topological materials, *Phys. Rev. B* **95**, 075146 (2017).
- [52] Liang Fu, C. L. Kane, and E. J. Mele, Topological Insulators in Three Dimensions, *Phys. Rev. Lett.* **98**, 106803 (2007).
- [53] Shou-Cheng Zhang and Jiangping Hu, A four-dimensional generalization of the quantum Hall effect, *Science* **294**, 823 (2001).
- [54] Dan S. Borgnia, Alex Jura Kruchkov, and Robert-Jan Slager, Non-Hermitian Boundary Modes and Topology, *Phys. Rev. Lett.* **124**, 056802 (2020).
- [55] Nobuyuki Okuma, Kohei Kawabata, Ken Shiozaki, and Masatoshi Sato, Topological Origin of Non-Hermitian Skin Effects, *Phys. Rev. Lett.* **124**, 086801 (2020).
- [56] Sebastian Weidemann, Mark Kremer, Tobias Helbig, Tobias Hofmann, Alexander Stegmaier, Martin Greiter, Ronny Thomale, and Alexander Szameit, Topological funneling of light, *Science* **368**, 311 (2020).
- [57] Tobias Hofmann, Tobias Helbig, Frank Schindler, Nora Salgo, Marta Brzezińska, Martin Greiter, Tobias Kiessling, David Wolf, Achim Vollhardt, Anton Kabaši, Ching Hua Lee, Ante Bilušić, Ronny Thomale, and Titus Neupert, Reciprocal skin effect and its realization in a topoelectrical circuit, *Phys. Rev. Res.* **2**, 023265 (2020).
- [58] T. Helbig, T. Hofmann, S. Imhof, M. Abdelghany, T. Kiessling, L. W. Molenkamp, C. H. Lee, A. Szameit, M. Greiter, and R. Thomale, Generalized bulk–boundary correspondence in non-Hermitian topoelectrical circuits, *Nat. Phys.* **16**, 747 (2020).
- [59] Chenwei Lv, Ren Zhang, Zhengzheng Zhai, and Qi Zhou, Curving the space by non-Hermiticity, *Nat. Commun.* **13**, 2184 (2022).
- [60] David M. Urwyler, Patrick M. Lenggenger, Igor Boettcher, Ronny Thomale, Titus Neupert, and Tomáš Bzdušek, Data and code for Hyperbolic topological band insulators, [10.5281/zenodo.6380568](https://doi.org/10.5281/zenodo.6380568) (2022).